Powder Technology 387 (2021) 385–395

Contents lists available at ScienceDirect

Powder Technology

journal homepage: www.elsevier.com/locate/powtec

Vibratory mixing of pharmaceutical powders on a single-tablet-scale

Andreas Kottlan [a], Benjamin J. Glasser [b], Johannes G. Khinast [a,c,*]

[a] Institute for Process- and Particle Engineering, Graz University of Technology, Inffeldgasse 13, A-8010 Graz, Austria
[b] Rutgers, The State University of New Jersey, Department of Chemical and Biochemical Engineering, 98 Brett Road, Piscataway, NJ 08854, USA
[c] Research Center Pharmaceutical Engineering GmbH, Inffeldgasse 13, A-8010 Graz, Austria

ARTICLE INFO

Article history:
Received 3 February 2021
Received in revised form 25 March 2021
Accepted 15 April 2021
Available online 20 April 2021

Editor: Aibing Yu

Keywords:
Personalized medicine
Vibratory mixing
Blending powder
Direct compression
Colorimetric concentration measurement

ABSTRACT

A single-tablet-scale mixing process, being part of a setup for the production of individualized tablets, is developed and studied. The process relies on the principle of vibratory mixing to achieve a homogeneous powder blend in the order of seconds. To investigate the mixing performance under various frequencies and amplitudes, a contactless evaluation method was implemented based on high-speed video recordings, a colored tracer and image analysis. The high spatial and temporal resolution of the recordings proved a valuable tool to assess the quality of the mixing process. Depending on the vibration parameters, different intensities of diffusive and convective mixing were observed. It was found that for similar accelerations, lower frequencies lead to faster mixing. Applying vibrational frequencies of 100 and 150 Hz and accelerations of 112 g a homogeneous blend of Emcocel 90 M and dyed Avicel PH-102 was produced within 2 s. This indicates the suitability of this approach for the use in the design of a small-scale direct compression process.

1. Introduction

The challenge of mixing powders affects a broad variety of industries. Examples include powder metallurgy [1,2], food preparation [3,4], propellant manufacturing [5] and pharmaceuticals [6–9]. In all those applications homogeneity of the powder mixture is the goal. In the pharmaceutical industry, solid dosage forms (which include tablets and capsules) are usually produced from a pre-blended powder. That means that the effective dose of an Active Pharmaceutical Ingredient (API) in a tablet or capsule is not only dependent on the correct weight of the API and all excipients in the bulk but also on the homogeneity after mixing. Consequently, various technologies have been implemented over the years to achieve the required mixing quality, as well as to prevent segregation after mixing. Segregation can either be prevented by granulation [10–12] or by designing a powder mixture and a process which minimize segregation potential if a direct compression process shall be realized [13,14]. A direct compression process, i.e., a process that does not involve any granulation steps, is the aim of the current study and the associated mixing step shall be closely investigated in the present work.

Direct compression has been widely adopted throughout the industry. Modern manufacturing techniques, such as continuous pharmaceutical production, often involve direct compaction, since the continuous granulation poses significant challenges. However, with respect to small-scale or individualized manufacturing, in the context of personalized medicine, many challenges remain. While personalized medicine has almost become state of the art in cancer treatment due to its very specific needs [15], its benefits are less exploited in other fields [16,17]. Such benefits are a higher therapeutic effect and less side effects by administering the specified amount of drug and better compliance/adherence by reducing the number of medicines a patient needs to take [18–20]. Also, for some diseases there is no constant dosing during the therapy and thus the ability to adjust the dose in each tablet for a prescribed therapy duration is desirable. The same is true for clinical studies in the context of adaptive pharmaceutics.

Therefore, we aim to develop a manufacturing process for small batches or individualized dose based on mixing (blending) and direct compaction. This process setup should bring us one step closer to what we consider as personalized medicine or a personalized medication manufacturing system. The process setup consists of the three fundamental steps of tablet manufacturing – dosing, mixing (blending) and compaction. A schematic which illustrates the setup is provided in Fig. 1. To guarantee the correct amount of API and excipients in each tablet, we will rely on a gravimetric dosing step, after which the circulating multipurpose vessel will be sealed and will remain sealed until the tablet has been compacted. Right after sealing the powder will be mixed to a

Abbreviations: API, active pharmaceutical ingredient; RAM, ResonantAcoustic® Mixer; g, acceleration of gravity;; NIR, near-infrared; ROI, region of interest; fps, frames per second; PIV, particle image velocimetry.

* Corresponding author at: Inffeldgasse 13/3rd floor, A-8010 Graz, Austria.
E-mail address: khinast@turaz.at (J.G. Khinast).

https://doi.org/10.1016/j.powtec.2021.04.040

Nomenclature

d_{50}	median particle diameter
d	inner diameter of the mixing vessel
h	height of the mixing vessel
$\hat{a}$	acceleration amplitude
y_0	half deflection amplitude
f	frequency
M	Lacey index
σ	current variance
σ_0	variance of a completely segregated system
σ_r	variance of a perfect random mixture
N	number of samples
w_t	mass concentration of tracer
$\overline{w_t}$	mean mass concentration of tracer
p	probability of finding a tracer particle
q	probability of finding a non-tracer particle
t	time
ξ	reduced travelled distance
r	red-value, equivalent to the a-value of the Lab color model

level of homogeneity enabling the production of a high-quality tablet. In the last stage the powder will be compacted into a tablet, which will then be ejected from the multipurpose vessel. This process design reduces the risk of segregation which commonly leads to problems with content uniformity in direct compression processes [21,22]. Furthermore, the temporal and spatial proximity of the mixing and the compaction step as well as the small volume of powder minimize the risk of segregation which could impact other critical quality attributes (CQAs) of the tablet. Each step bears the possibility to adjust process parameters based on the composition of the tablet, being produced. In the pursuit of reaching a practicable output rate we set a limit of around 10 s for the whole process. Optimization and parallelization can then lead to a setup for use in hospitals, nursing homes, special pharmacies, and other remote applications.

As mentioned above, in the present work we will focus on the mixing (blending) step of this process and especially on the quantification of the mixing quality. The goal is to achieve mixing of 200 to 1000 mg of powder to an acceptable homogenous state in a sealed container within less than 10 s. The homogeneous mixing of polydisperse powders poses a significant challenge in the development of pharmaceutical manufacturing processes. These challenges do not only emerge from differences in size [23–25] but also from different densities [26] and shapes [27] as well as from cohesive effects [28]. Those influencing parameters require insight into the mixing process to overcome limitations in blending capability. Based on that insight a proper selection of a mixing device can be made. Traditional mixers can be split in two categories – those using stirring elements, such as convective, impaction and high shear mixers and those where the shell moves or rotates such as tumbling mixers [29]. For granular systems showing segregation tendency, convective mixing was found more effective [25]. Convective mixing is predominant in mixers using stirring elements. As we aim to keep the vessel sealed after dosing, inserting, and removing of a stirring element was in conflict with the specifications. However, a tumbling mixer would not be able to readily overcome cohesive forces of many pharmaceutical powders due to the small masses involved in the process.

Therefore, we use a different approach, i.e., acoustic, or vibratory mixing. The principle is depicted in Fig. 2. As illustrated, the powder bulk is exposed to vibrations, leading to agitation of the bed. Depending on acceleration magnitude, frequency and powder characteristics either mixing or segregation can be observed. The most famous example for the latter might be the Brazil nut effect driving large particles to the surface of powder beds. A summary of size segregation mechanisms is provided by Schröter et al. [30]. Besides segregation or mixing, vertically shaken powders show various types of behavior, ranging from bouncing beds, to undulations, the granular Leidenfrost effect, convections cells or the state of a granular gas. Which of these states is observed depends on the frequency, the acceleration magnitude, the number of layers within the powder bed and cohesive effects [31,32]. The right combination of parameters can therefore lead to efficient mixing exhibiting the characteristics shown in Fig. 2 [33,34], where the interactions of the large-scale and small-scale mixing effects leads to a breakdown of segregated structures. While most experimental studies deal with quasi-2D systems [31,32,35,36], we investigate a system contained by a cylindrical tube, representing the geometry of the multipurpose vessel we intend to use for the tablet manufacturing process. Promising results for the vibratory mixing of pharmaceutical powders are provided by Osorio et al. [37,38] who use a ResonantAcoustic® Mixer (RAM) (Resodyn Acoustic Mixers, Butte, Montana, USA) capable of generating a resonant frequency of ~60 Hz and accelerations of up to 100 g (where g = acceleration of gravity). They investigated the influence of fill level, mixing time and acceleration magnitude on the Relative

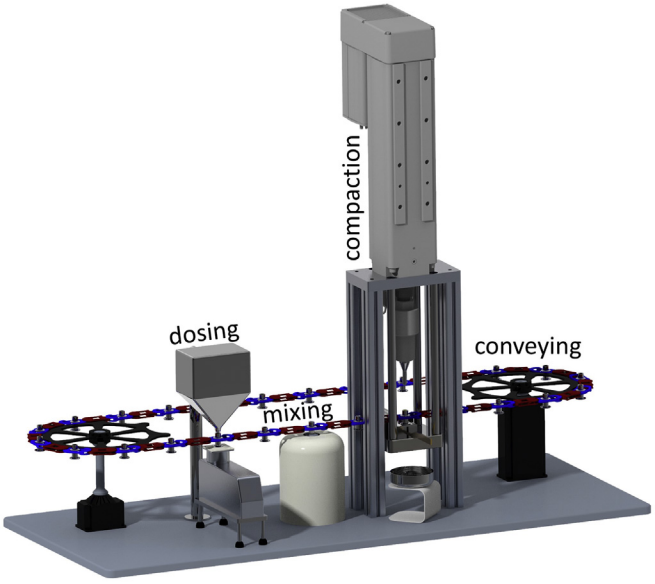

Fig. 1. Process setup for individual on demand tablet manufacturing, consisting of a dosing-, mixing- and compaction-stage as well as a connecting conveying system. (For interpretation of the references to colour in this figure legend, the reader is referred to the web version of this article.)

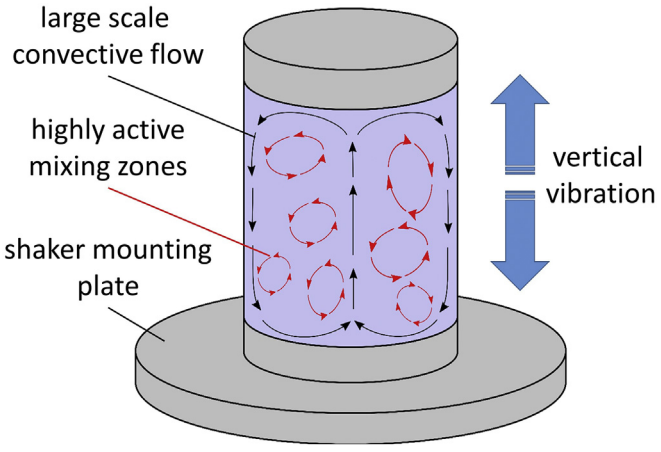

Fig. 2. Schematic illustration of the mechanisms leading to homogenization in a vibrational mixing process. (For interpretation of the references to colour in this figure legend, the reader is referred to the web version of this article.)

Standard Deviation (RSD) and the temperature rise for the model APIs acetaminophen and caffeine blended with different excipients. A successful application of this technology was also reported by Tanaka et al. [34] in a comparison of a RAM and a traditional V-blender. As we aim to mix masses of up to only 1000 mg we have observed it is possible to reach the desired level of acceleration without exploiting resonance effects. Therefore, the mixing behavior at different frequencies has been investigated at accelerations of up to 110 g. The small system size in our work yields the additional advantage of a shorter mixing time by reducing the size of the initially segregated volumes.

For the assessment of mixing quality, several challenges arise including (1) representative sampling [39], (2) measuring the (low) concentration of a component of interest within a (small) sample [40] and (3) the mathematical description of the degree of mixedness [41–44]. Using optical concentration measurements (since actual sampling would be extremely challenging) has the intrinsic drawback of only analyzing the observable surface of the powder bulk, which is the main challenge with respect to representative sampling. An advantage in terms of representative sampling can be found by choosing sampling regions (position and size) after image capturing in an iterative process, to obtain the best representation. The ability to represent the whole powder bed using this sampling method will be discussed in Section 3.3.

With respect to the second challenge, the small size of the system limits the number of applicable sampling methods. The use of a 1 ml sample-thief [45] combined with near - infrared (NIR) chemical imaging was not a good option. Also the application of an in-line NIR-probe [46] would yield an average concentration for the analyzed area. These limitations and the desire for a high time resolution suggest the use of a high-speed camera and a colored tracer. High-speed image recording provides the advantage of a high temporal and spatial resolution, enabling different means of evaluation. Based on calibration samples a correlation between color intensity and tracer concentration in a specified image area can be made. A colorimetric approach on concentration measurement was successfully applied by Emady et al. [47] for 80 μm fluidized-bed cracking catalyst particles, which is in the particle size range of the powders we aim to investigate. Emady et al. used a colorimeter to determine the color and tracer concentration of the analyzed samples. While colorimeters, also known as spectrophotometers, combine lighting and measurement of the reflected light, a setup using a CMOS-camera relies on an external light source. Based on different ambient lighting, the light reflected from the sample changes its color. To enable a quantitative concentration measurement, calibration and experiments have to be done under the same lighting conditions using a fixed white balance. Concentration measurements based on a 3-color CCD-camera proved a valuable tool for concentration measurement in flow through experiments of saturated porous media [48]. Equivalent performance of a colorimetric and a fluorescence approach in the measurement of tracer concentration in a pharmaceutical capsule filling process was reported by Scheibelhofer et al. [49].

In the present study the applicability of a vibratory system on small-scale mixing of pharmaceutical powders and the suitability of high-speed video analysis, for the evaluation of such a process, are investigated. After describing the materials, we present the setup for mixing powders on a single-tablet-scale at various frequencies at acceleration amplitudes up to 110 g. Then, techniques for the image-based mixing analysis, as well as for the characterization of the shaking device, are presented. To provide a quantitative measure for vibratory mixing, we introduce an alternative metric to the mixing time for vibratory mixing analogously to the number of revolutions in a rotary or tumbling mixer. The results of shaker characterization, calibration and mixing analysis will be discussed in the results section. Finally, we conclude with a discussion of the preferred mixing frequencies and consider the capabilities and limitations of the mixing analysis.

2. Materials and methods

2.1. Powders

Two pharmaceutical powder materials were used. As the aim was to develop a technique to assess mixing quality on a visual basis no APIs were used. This was done as a first step in order to demonstrate proof-of-concept without the safety concerns of working with APIs. The focus was on pharmaceutical relevance and the suitability for dyeing the powders with a water-soluble coloring agent. Therefore, we chose two microcrystalline celluloses (MCC), i.e., Emcocel 90 M (E-90) and Avicel PH-102 (A-102) having a nominal mean particle size of 90 μm and 100 μm respectively [50]. Both powders are widely used as fillers and binding agents in direct compression formulations. They show good disintegration behavior and lead to high tensile strength in tablets even at low compaction pressures [13,50].

The optical difference between the two materials was achieved by using as-received Emcocel 90 M (JRS Pharma LP, Rosenberg, Germany) and Avicel PH-102 (FMC Biopolymer, Philadelphia, United States) dyed with red food color (No-taste Red Icing Color, Wilton Industries, USA), see Fig. 3. The optical microscope images in Fig. 3 show a higher content of needle-shaped particles in Emcocel than in the dyed Avicel, which is also reflected in their flowability.

The flowability of both powders was characterized using an FT4 powder rheometer (Freeman Technologies, Tewkesbury, United Kingdom), while the Hausner-Ratio was determined using a tap density tester PT-TD200 (Pharma Test Apparatebau AG, Hainburg, Germany). The flow function as well as the conditioned bulk density was determined using the standard shear cell procedure provided by Freeman Technologies at a normal stress of 3 kPa using a 25 mm shear cell. The flow energy measurement was conducted using a 25 mm

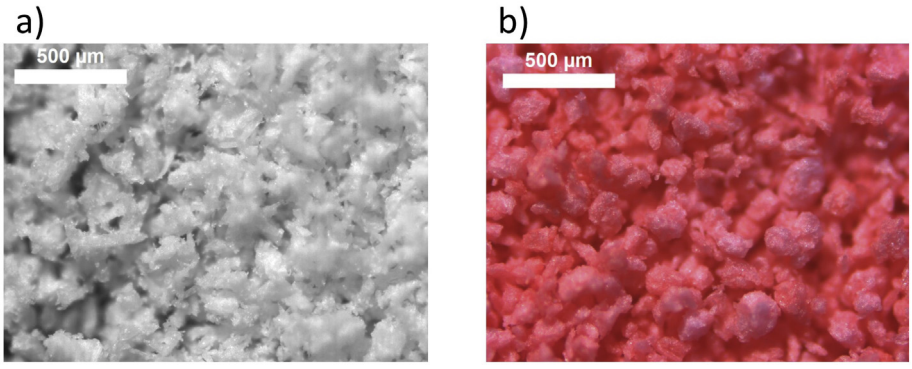

Fig. 3. Optical microscope images of (a) Emcocel 90 M and (b) dyed Avicel PH-102, i.e., the tracer. (For interpretation of the references to colour in this figure legend, the reader is referred to the web version of this article.)

Table 1
Properties of the materials.

	d_{50} (μm)	Conditioned bulk density (kg/m^3)	Flow energy (mJ)	Hausner Ratio (−)	Flow function @ 3 kPa (−)
Emcocel 90M	126.0	370.0	255	1.43	9.0
Avicel PH-102 dyed	118.2	367.5	169	1.36	10.3

vessel combined with a 23.5 mm helix blade, according to the respective Freeman technologies standard procedure. Table 1 shows the measured d_{50}, conditioned bulk density, flow energy, Hausner Ratio and the flow function of the powders. The system investigated in the mixing experiments was a 50:50 mixture of Emcocel 90 M and Avicel PH-102, yielding a d_{50} of 122.1 μm for the binary mixture.

2.2. Measuring setup

To analyze the mixing progress, of the materials being exposed to vertical vibrations the setup shown in Fig. 4 was used. The mixing vessel itself can be seen in Fig. 5. As no compaction of the powder is done in the present study, a transparent PMMA tube with an inner diameter of 10 mm was used to contain the powder which enabled us to observe the particle motion. An anti-static spray was used to coat the inner surface of the tube, to minimize the number of particles sticking to the surface. At the top and the bottom, the powder is enclosed by two aluminum parts yielding an inner height of 17.5 mm (see Fig. 5). The black O-rings do not only seal the container but also maintain the position of the aluminum parts during vibration. On the bottom part a threaded bolt is used to screw the container to the platform of the electrodynamic shaker (TIRA TV 51120, Tira GmbH, Germany) which is based on a moving coil principle. The movement of the shaker is created by a sinusoidal signal of the function generator (PeakTech Prüf-und Messtechnik GmbH, Germany) which is amplified by an analog amplifier (BAA 500, Tira GmbH, Germany). For all mixing experiments, a sine wave was chosen for excitation of the shaker and the amplitude of the function generator was set to 5 Volt. The amplifier was set to voltage mode at the maximum amplification factor.

Image acquisition was realized using a high-speed camera (Phantom VEO640L, Vision Research, Wayne, New Jersey, USA). Adequate lighting is provided by a 100 W LED spotlight. In order to track only the motion of the powder bed and not the motion of the whole container, the frequency of image capturing is synchronized with the vibration frequency. This means that for example for a vibrational frequency of 150 Hz, 150 images are taken per second. To make as much information

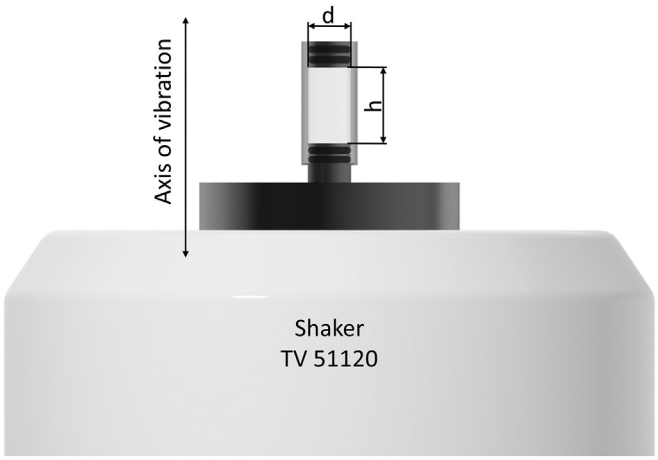

Fig. 5. Mixing vessel consisting of aluminum lid and base and a PMMA tube; including O-rings (black) maintaining the position of parts during vibration. The assembled mixing vessel is screwed to the mounting plate of the electrodynamic shaker TV 51120 (Tira GmbH, Germany); d = 10 mm, h = 17.5 mm.

accessible as possible, we recorded the images in the maximum available color depth of 12 bit. The original image resolution was 2560 × 1600 pixels, from which a Region of Interest (ROI) of 850 × 480 pixels was cropped for image analysis. Exposure time was set to 10 μs, to prevent motion blur, independent of vibration- and image acquisition frequency.

2.3. Shaker characterization

As the shaker is the heart of the vibratory mixing process, the oscillatory motion was analyzed, as well as the mechanical suspension of the moving coil which changes the ideal sinusoidal wave provided by the electrodynamic setup.

2.3.1. Motion analysis

Since additional mass reduces the maximum acceleration provided by the electrodynamic shaker, no acceleration sensor was attached to the shaker platform during the experiments. Instead, the movement of the mixing vessel was analyzed using visual motion tracking. A monochromic camera (Os 8 S3, IDT – Integrated Design Tools, Inc., Pasadena, USA) was used for motion tracking experiments. The recorded images were evaluated using the motion tracking tool of the software Motion Studio (IDT – Integrated Design Tools, Inc., Pasadena, USA). Since the

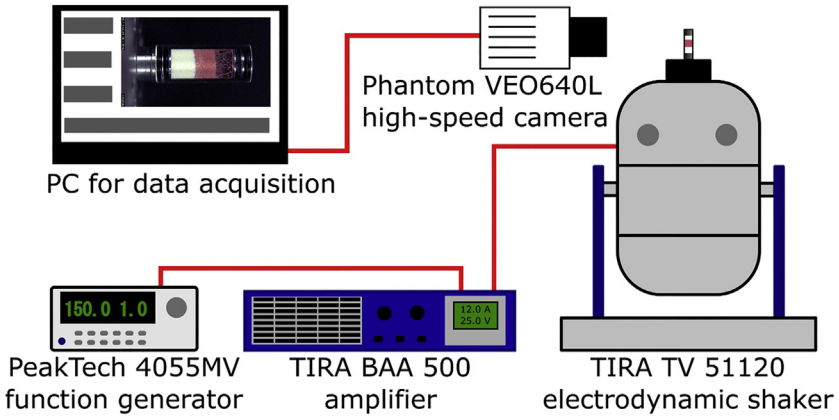

Fig. 4. Experimental setup for execution and recording of powder mixing experiments. (For interpretation of the references to colour in this figure legend, the reader is referred to the web version of this article.)

function generator provides a sine wave the maximum acceleration $\hat{a}$ can be calculated by $\hat{a} = y_0 \cdot 4\pi^2 f^2$, with y_0 being the amplitude and f the frequency of vibration. While y_0 is accessible through the motion tracking data, f is fixed by the provided signal. To reach a satisfactory resolution of the motion signal, a frame rate of 6000 fps was used. The position data yielded by the motion tracking is then fitted by a sine wave using Microsoft Excel (Microsoft, Redmond, USA) to extract the amplitude of the vibrational movement.

2.3.2. Force-deflection-measurement

To investigate the influence of the mechanical suspension in the shaker system, a force-deflection-measurement was executed. The measurement was realized with an electric linear actuator with an integrated load cell (RCS3-RA4R, IAI, Shizuoka Prefecture, Japan). Using the manufacturer's PC-interface and software, position and force data were recorded with a frequency of 1 kHz. To account for dynamic behavior, velocities of 1, 5, 10 and 50 mm/s were applied using the linear actuator. As the load cell setup is solely designed to measure thrust, only deflection in the negative vertical direction was examined. For each velocity, the deflection was set to 8 mm. The measurement was repeated 5 times for every velocity setting.

2.4. Image analysis

The images captured by the color high-speed camera were analyzed using the software Matlab as well as the toolboxes DIPimage(Quantitative Image Group, TU Delft, Netherlands) and EzyFit [51]. To uncouple the influence of brightness and color, the images were transformed from the RGB to the Lab color space. The Lab color model describes the color of a pixel by L – the Lightness, a – a hue value ranging from the positive extreme for red and to the negative for green and b which describes the same for yellow (positive) and blue (negative). This enables us to analyze the intensity of red color within the powder bed individually by looking at the a-value. This is why it is called red-value below. An image is then represented by an X x Y x 3 matrix were X x Y is the image size in pixels. Each of these matrix coordinates has then 3 values, i.e., the L, a, b value, assigned to it. As this can be viewed as an image consisting of three intensity layers, one can pick a single layer for analysis, just as we did with the second layer, the a-layer. To get rid of lighting inhomogeneity, in the images used for visualization, a reference image is created from 150 images of pure Emcocel in motion. Afterwards the L matrix of each image is divided by the L matrix of this averaged reference image and multiplied by the mean of the reference image. An influence of lighting on the red-value was not visible, therefore no correction of the red-value was done.

2.4.1. Calibration

To correlate the tracer content and the measured red-value in an image, a calibration procedure was performed. For calibration, 7 mixtures containing 0, 20, 40, 50, 60, 80 and 100% were prepared and mixed with the setup depicted in Fig. 4 at a frequency of 150 Hz and an acceleration of 110 g. The exact masses used for calibration are stated in Table 2. The mixing process was recorded using the high-speed camera at a frame rate of 30 fps. For calibration, the averaged mean red-values of 60 images recorded after 2 s of mixing were used. The calibration images were recorded while the powder was in motion, to reflect the same conditions in terms of powder bed density and therefore color intensity as in the experiments. The ROI was chosen to be the same size as for the mixing analysis. A continuous correlation was created by fitting a 3rd order polynomial to the data using EzyFit.

Table 2
Composition of samples used for the calibration of the red-value response to tracer concentration.

	Comp 1	Comp 2	Comp 3	Comp 4	Comp 5	Comp 6
Mass of Emcocel 90 M [mg]	400	320	240	159	79	0
Mass of dyed Avicel PH-102 [mg]	0	80	161	241	321	400
Real tracer content [%]	0	20.00	40.15	60.25	80.25	100

2.4.2. Mixing analysis

The powder mixtures we aimed to prepare were 1:1 mixtures of Emcocel 90 M and dyed Avicel PH-102 tracer. A way of describing the state of segregation in a system has been the subject of research [52,53]. In this work we chose the Lacey index [42] as the general metric to describe the mixing quality within the powder blend [54,55]. As the extent of segregation of the powder blend has a high impact on the critical quality attributes of the manufactured tablets, we decided to evaluate the size of striations as done by Kukukova et al. [44]. The relative areas of striations consisting of one component (purity >80%) are analyzed. The size of striations is relevant as it directly reflects the size of segregation patterns, which is of high importance as segregation limits the mechanical stability of a tablet.

To calculate the Lacey index M, 16 sample spots were defined, i.e., eight in the lower half, eight in the upper half of the powder bed. The exact location can be seen in Fig. 6a. The mean concentration of tracer within one sampling box is then determined by calculating the mean red-value and converting it to a concentration using the calibration function. From those values the Lacey index is then calculated as shown by Eq. 1, 2 and 3. Here, σ_0 is the variance of a totally segregated system, σ_r the variance of a perfectly randomly mixed system and σ the actually measured variance in the system, N the number of samples, w_t the measured mass concentration of tracer at a sampling spot, $\overline{w_t}$ the mean mass concentration of tracer in the system, p the probability of finding a tracer particle and q the probability of finding a non-tracer particle when sampling. As can be seen, the real and not the empirical variance and mean concentration, are used. This allows us to identify if only the visual surface is homogenous or if the whole volume is mixed homogenously and is possible as we know the true mean for each experiment. Since we analyze a poly-disperse powder and use averaging to evaluate the concentration at a sampling spot, theoretically a perfect mixture can be achieved. Therefore, we chose $\sigma_r = 0$.

$$M = \frac{\sigma_0^2 - \sigma^2}{\sigma_0^2 - \sigma_r^2} \tag{1}$$

$$\sigma^2 = \frac{1}{N} \sum_{i=1}^{N} (w_t - \overline{w_t})^2 \tag{2}$$

$$\sigma_0^2 = p \cdot q \tag{3}$$

To calculate the maximum relative striation area, the threshold and labeling function of DIPimage were used. Threshold values based on calibration data were introduced to identify areas of more than 80 or less than 20% tracer content. All continuous areas fulfilling this criterion receive a label and their size is measured. To arrive at the relative maximum striation area, the largest area value is divided by the overall area of the ROI. Fig. 6b-d show an image recorded prior to mixing and at its labeled counterparts for <20% (c) and >80% (d) tracer content. The same is visible in e-g for a mixing time of 0.7 s at 150 Hz and approximately 112 g.

To compare the progress of mixing at different frequencies, we introduce the reduced travelled distance ξ which is defined as $\xi = t \cdot f \cdot 2 (y_0 - d_{50})/h$ with t being the mixing time, f the vibration frequency, y_0 the vibration's amplitude in one direction, while d_{50} reflects the particle size of the powder mixture and h the height of the mixing vessel. ξ should describe the cumulative bed agitation and accounts for the mobility of the particles due to the vibration amplitude and their size. This metric is intended to be equivalent to the number of revolutions in a

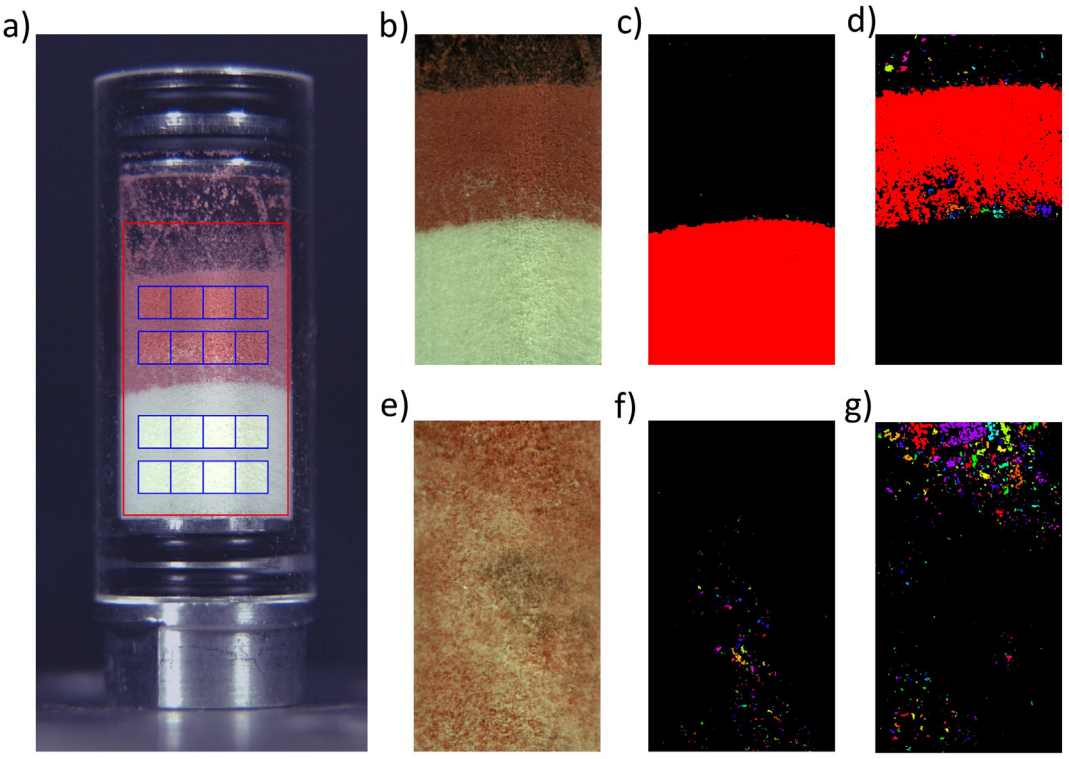

Fig. 6. a) original image recorded by the high-speed camera indicating the Region of Interest for striation analysis (red boundary) as well as the sampling spots used for the calculation of the Lacey-index (blue squares). b) ROI of an original image recorded prior to mixing. c) labeled image corresponding to areas in b) with a tracer concentration below 20%. d) labeled image corresponding to areas in b) with a tracer concentration above 80%. e) ROI of an original image recorded after 0.7 s of mixing at 150 Hz. f) labeled image corresponding to areas in e) with a tracer concentration below 20%. g) labeled image corresponding to areas in e) with a tracer concentration above 80%. (For interpretation of the references to colour in this figure legend, the reader is referred to the web version of this article.)

rotary or tumbling blender. In the contrast to rotary mixing, the number of oscillations is not practical, as in contrast to revolutions in a rotary mixer there is no direct coupling between number of oscillations and cumulative bed agitation.

2.5. Experimental design

As indicated by previous studies, certain combinations of frequency and amplitude are needed to lead to satisfactory mixing. As the study by Osorio et al. [37] suggests that higher acceleration leads to faster mixing, the highest acceleration achievable with the setup was used for this work, being ~110 g. Regarding the adopted frequency some preliminary tests were executed. Based on these tests, the frequency range was set to 100–300 Hz. The lower limit is due to the limited deflection of the shaker which does not allow for maximum accelerations below 100 Hz. 300 Hz were chosen as upper limit, as frequencies above showed decreasing agitation of the bed, because of the small amplitude. The investigated powder mass was fixed at 400 mg representing a single tablet of 400 mg with an API dose of 200 mg.

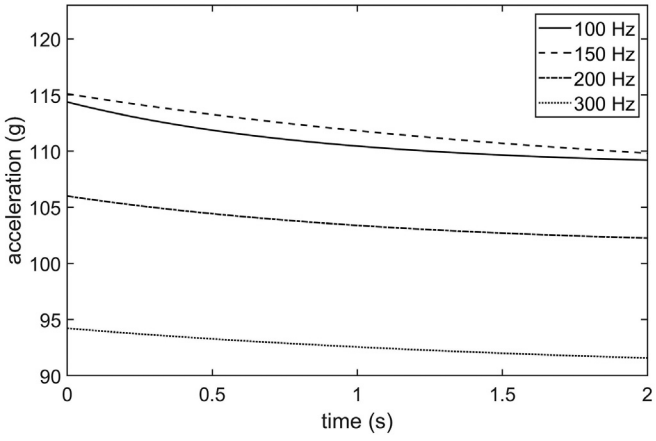

Fig. 7. Evolution of the acceleration amplitude of the vibrational motion during the onset of the mixing process.

3. Results and discussion

3.1. Vibration analysis

Despite the fact that the function generator's amplitude and the amplification were set to constant values for all investigated frequencies, different acceleration amplitudes were observed, as can be seen in Fig. 7. Lower frequencies led to higher initial acceleration amplitudes. Additionally, a decrease over time was observed for all frequencies. Closer investigation of the position data showed, however, a good correlation between the real oscillation and the ideal sinusoidal wave form used for excitation. The differences between different frequencies might be explained by two factors influencing the actual vibrations:

Table 3
Offset and deflection amplitudes for the investigated frequencies.

	Offset [mm]	$y_{0,0}$ [mm]	$y_{0,2}$ [mm]	a_{spring} [m/s^2]
100 Hz	3.60	2.845	2.680	7.71
150 Hz	0.92	1.278	1.184	3.46
200 Hz	0.54	0.662	0.633	1.79
300 Hz	0.22	0.260	0.250	0.70

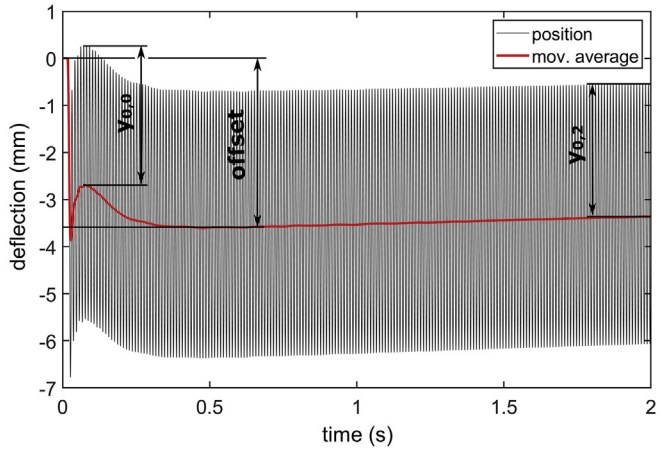

Fig. 8. Deflection measurement for 100 Hz experiment. (For interpretation of the references to colour in this figure legend, the reader is referred to the web version of this article.)

The first one is the mechanic suspension of the shaker's moving coil. To maintain a stable position at rest, the coil is suspended on eight cantilever springs. Those also act as radial bearing to keep the moving coil centered. This suspension adds a force to the magnetic force created by the sine wave signal. The added force is higher for high deflections which occur at low frequencies. While this explanation agrees with the trend observed while going from 150 to 300 Hz, it does not explain that accelerations at 100 Hz are similar to those at 150 Hz. The reason might, to a part, be the offset from the initial rest position and the neutral position during the oscillatory movement. At the excitation voltages we used in the present study, for different frequencies a different offset is observed. This offset, as well as the initial deflection amplitude $y_{0,0}$ and the deflection amplitude after 2 s $y_{0,2}$ are provided in Table 3, while their meaning is illustrated in a deflection over time diagram in Fig. 8.

The force-deflection-measurement of the mechanical suspension showed that the mechanical suspension behaves like a 2-step linear spring with a force constant of 6.3 N/mm for deflections lower than 3.6 mm and a force constant of 7.05 N/mm for deflections between 3.6 and 8 mm. Using these force constants, the influence of the offset and the amplitude on the peak acceleration was calculated. The portion of acceleration emerging from the springs is stated in Table 3 as a_{spring}.

The second effect which might influence the performance of the shaker is that of magnetic losses in the moving coil when its polarity is changed. The shaker's main resonance frequency is reported to be at 6500 Hz by the manufacturer. Hence, resonance should not influence the motion for the investigated frequencies. Comparing the acceleration amplitudes and the influence of the mechanical suspension suggests that the dominant influence comes from electrodynamic effects.

The decrease of the amplitude over time can be explained by the temperature rise in the coil during operation. As the amplifier is providing a constant peak voltage, the electric current decreases with increasing resistance due to the rising temperature. This leads to a lower force available, for accelerating the moving coil and the mixing vessel.

3.2. Calibration

The red-values r yielded by image analysis of mixtures with known tracer content w_t are indicated by the black circles in Fig. 9. As can be seen, there is no linear correlation between tracer concentration and red-value. To account for this a 3rd order polynomial was fitted to the measured data. The fit is depicted as black line in Fig. 9 and is described by Eq.(4).

$$w_t = 28.953 + 2.6283 \cdot r + 3.1142 \cdot 10^{-2} \cdot r^2 - 1.3058 \cdot 10^{-3} \cdot r^3 \quad (4)$$

As the fit decreases to values below zero for red-values between approximately −22 and −16, a criterion is introduced to prevent negative values for tracer concentration, leading to the final form (Eq. (5)):

$$w_t = max\left(0; 28.953 + 2.6283 \cdot r + 3.1142 \cdot 10^{-2} \cdot r^2 - 1.3058 \cdot 10^{-3} \cdot r^3\right) \quad (5)$$

Eq. (4) depicts the calibration data points with a correlation coefficient R of 0.9998. It is defined as $R^2 = SS_{reg}/SS_{tot}$, where $SS_{reg} = \Sigma\left(y_{fit} - \bar{y}\right)^2$ and $SS_{tot} = \Sigma(y - \bar{y})^2$ with y_{fit} being the fitted values $\bar{y}$ the mean of the measured values and y the measured values.

The evolution of the red values over time is shown in Fig. 10 for various tracer concentrations. As can be seen, strong fluctuations at the beginning are observed. After some time, a plateau seems to be reached, yet some fluctuations are still observed except for the case with no tracer. The red values of all mixtures increase, except for the one with pure systems. The fluctuations can be explained by the fact that only the surface of the powder bed is observed. For 100% tracer, abrasion of the particles, creating colorless fines, is the reason for

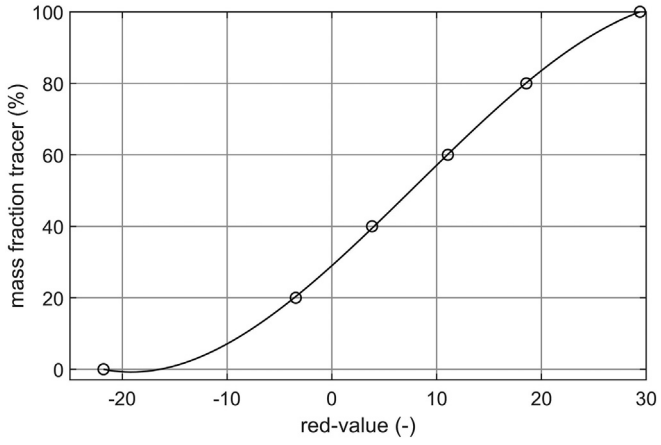

Fig. 9. Tracer mass fraction in the mixtures used for calibration vs. the measured red-values (circles). The solid line indicates the polynomial fit of third order (Eq. (4)).

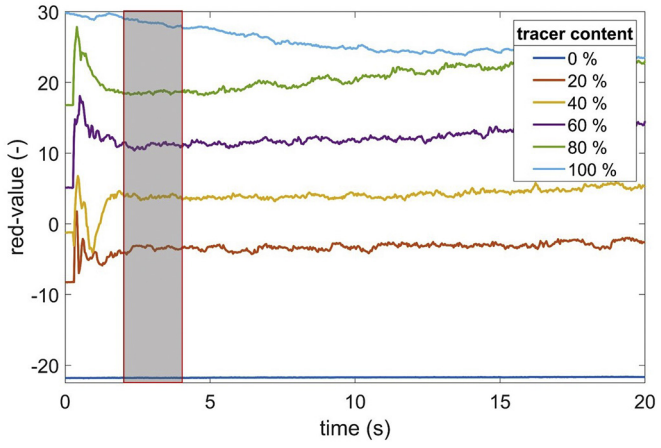

Fig. 10. Red-value measured in the calibration samples over time during vibration at 150 Hz and 110 g. The grey area indicates the timespan used for averaging. (For interpretation of the references to colour in this figure legend, the reader is referred to the web version of this article.)

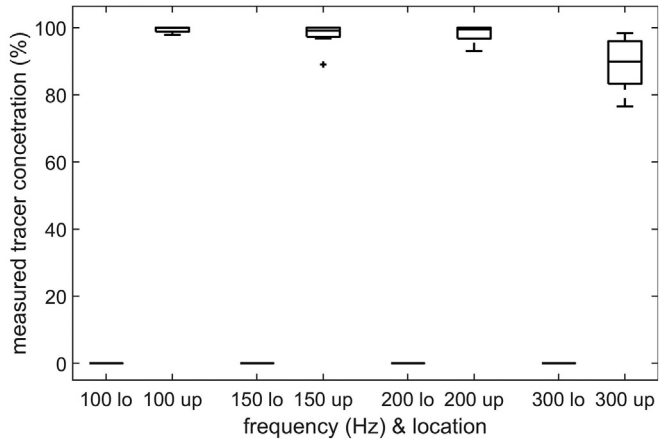

Fig. 11. Tracer concentrations measured at the initial state for each experiment in the lower and upper half of the mixing vessel.

decreasing red-values. In addition, the red values are also influenced by clouding of the transparent tube by fines.

The applicability of the calibration to the images of the mixing experiments was tested by evaluating the tracer content at the upper 8 and lower 8 sample spots (according to Fig. 6a) before the mixing process started.

Fig. 11 shows a boxplot which depicts the tracer content in the lower and upper half of the container. As can be seen the tracer content is correctly measured for all initial states as zero in the lower half, while there are small deviations from 100% in the upper half for the initial state for 100, 150 and 200 Hz. For the 300 Hz experiment larger deviations from the expected value are seen for the upper half. This deviation can be explained by the filling order. When filling the powder into the container, particles attach to the wall due to electrostatic forces, despite the use of an anti-static spray to coat the inner surface of the tube. Therefore, white particles are also in the upper half, while there are no red ones in the lower half.

3.3. Mixing analysis

Images of the ROI for 100, 150, 200 and 300 Hz are presented in Fig. 12, while the respective videos are available below (100 Hz – Video 1, 150 Hz – Video 2, 200 Hz – Video 3, 300 Hz – Video 4). They highlight the effect of different frequencies on mixing of the materials. Furthermore, the main phenomenon leading to differences in the mixing efficiency, which is the size of the intense-mixing zone (or zones if there are more of them) can be seen.

Intense-mixing zones are zones within the powder bed exhibiting a lower density and higher particle velocities. While they cannot easily be distinguished in the images, they are clearly visible in the video recordings. These mixing zones lead to homogenization by strongly enhancing diffusive mixing and by the convection induced in denser regions of the powder bed. Regardless of the frequency, we observed that the formation of dilute intense-mixing zones starts at the top of the bed. In these intense-mixing zones the powder behaves like a granular gas, as it is observed for shallow granular beds at lower accelerations [31]. Since the intense-mixing zones support the weight of denser regions within the bed, a similarity to the granular Leidenfrost effect as observed by Eshuis et al. [31] can be identified.

For 100 Hz a mixing zone can be observed that starts to form at the top and then in the course of time spreads over about 70% of the container leading to fast mixing. As the height of the white layer decreases and no change in color of the red layer is observed until 0.15 s, we assume it moves upwards on the backside of the container to come down at 0.2 s. From 0.3 s on we observe an almost perfectly mixed system.

In the second row in Fig. 12 showing the experiment at 150 Hz, we can identify one smaller mixing zone developing in the top-right corner. Together with at least one other mixing zone it produces an additional convective flow, conveying powder upwards in the middle of the container. The combination of these two phenomena is responsible for mixing at this frequency.

If the powder is excited by 200 Hz we observe smaller mixing zones which also “travel” more slowly through the powder bed. The same can be seen for 300 Hz with even smaller mixing zones. For 300 Hz a layered

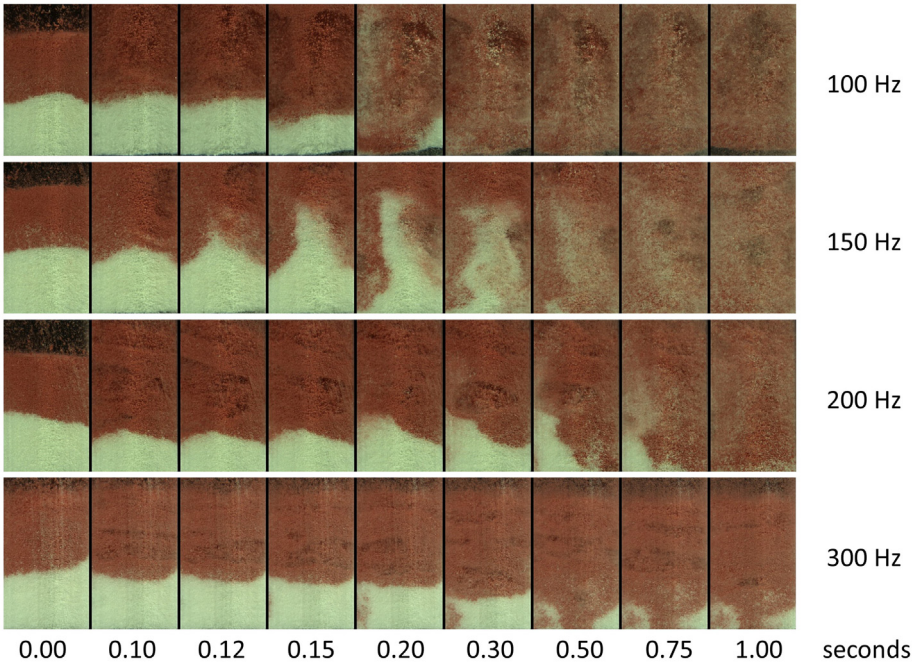

Fig. 12. Images recorded during the mixing process showing the progress of mixing. (For interpretation of the references to colour in this figure legend, the reader is referred to the web version of this article.)

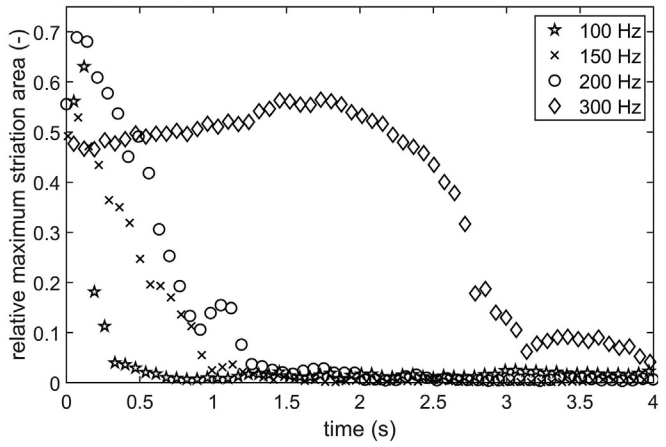

Fig. 13. Relative maximum striation area below 20 or above 80% tracer concentration versus mixing time.

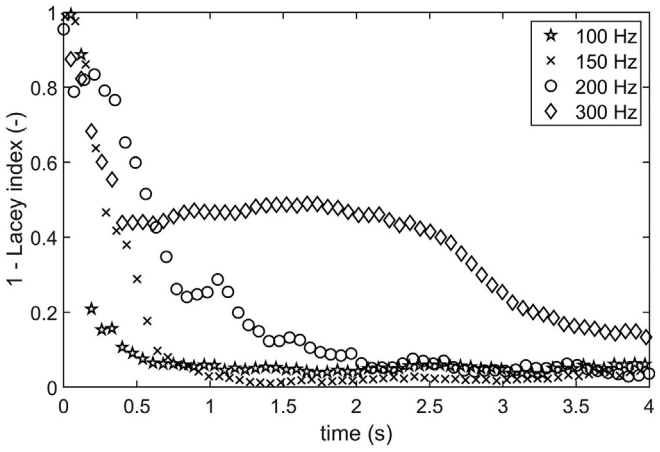

Fig. 14. (1 – Lacey index) versus mixing time for the investigated frequencies.

structure of dilute horizontal mixing zones and dense powder can be observed. Convective flows seem to emanate at the front towards the back of the container, as the undyed Emcocel disappears from view. Furthermore, a higher amount of fines stuck to the transparent container's wall at 300 Hz, which might not have been directly linked to the frequency, but influenced the colorimetric concentration measurement. This clouding effect is clearly visible in Video 4.

Despite the attachment of fines at the surface of the tube, particle movement is still clearly visible. The migration of particles between the visible surface and the inside of the bed is observable in the videos (Videos 1–4) regardless of the frequency. This indicates a sufficient representation of the mixing quality inside the powder bed volume by observing the visible surface. We should however note that all our results are based on the visible outer surface of the vessel and we can only infer flow inside of the bed. Further work with a sophisticated experimental technique like PEPT is needed to examine the three-dimensional flow dynamics inside the bulk of the bed.

The quantitative analysis of the size of the striations is provided in Fig. 13. As can be seen, the relative maximum size of striations decreases for all cases and reaches 0 after a maximum of 2 s except for 300 Hz. From Fig. 13 it can be seen that the mixing speed decreases for increasing frequency. The increase of the striation area for 200 Hz starting at about 1 s indicates the coalescence of multiple striations and therefore temporary segregation. At 300 Hz the mixing process is significantly slower, as indicated by an increasing size of the striation area until about 2 s. A comparison of the relative maximum striation area and the images (Fig. 12) for 300 Hz shows a difference between visual perception and the results yielded by analysis based on threshold images. One reason is the diffusive mixing which decreases the purity of the tracer slightly below 80% which is not visible with the bare eye. The other reason is the fact that the bed does not expand to the full area of the ROI used to calculate the relative value.

Fig. 14 shows one minus the Lacey index M on the y-axis to make a comparison to the striation area easier. 1-M can also be viewed as a segregation index. The use of the Lacey index provides better distinction between the progress of mixing for 150 and 200 Hz. It indicates the same mixing quality for 100 and 150 Hz earlier than the size of segregation measurement which also fits the impression gained by visual examination of the images. Although the powder seems almost homogenously mixed at 1 s for 200 Hz the Lacey index as well as the size of segregations suggest that the mixing process is not yet completed.

Fig. 15 presents 1-M over the reduced travelled distance ξ. As the different amplitudes of the vibrational motion for different frequencies are considered in the calculation of ξ, the mixing progress can be viewed as only depending on the reduced travelled distance. As can be seen for 100 and 150 Hz, the mixing-versus-travelled distance plots almost collapse into a single curve. Due to the temporarily stagnating mixing progress for 200 and 300 Hz there is some deviation from the trend. Still the curves show a similar slope as the other two when there is progress.

Because of the good correlation of the mixing progress for 100 and 150 Hz, we propose, that for the vibrational mixing of a specific powder applying the same acceleration amplitude in the same geometrical setup the mixing progress can – with limitations – be described solely using the reduced travelled distance. ξ can therefore be viewed analogously to the number of revolutions in a rotary or tumbling mixer which is commonly used instead of the time as this allows to compare mixing processes regardless of the rotational speed. The fit is given by Eq. (6).

$$1-M = 0.03 + \exp\left(-0.24\cdot(\xi-1.143)\right) \tag{6}$$

The fit is shown as red line in the figure. The good correlation between the fit and the results for 100 and 150 Hz shows that the decrease of segregation can be described by an exponential law using ξ. This fit is of course only applicable if no stagnations in the mixing progress occur, which apparently happens at higher frequencies and thus lower amplitudes. Stagnations like the ones that were observed seem to occur if the size or number of intense-mixing zones is too small to link two segregated areas. If an intense-mixing zone is smaller than a

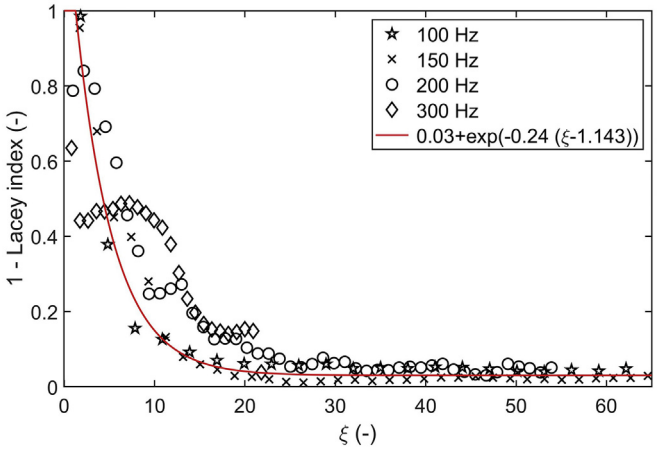

Fig. 15. (1 – Lacey index) versus the reduced travelled distance ξ (black markers). Exponential fit representing the decrease of segregation resulting from the investigated mixing process (red line). (For interpretation of the references to colour in this figure legend, the reader is referred to the web version of this article.)

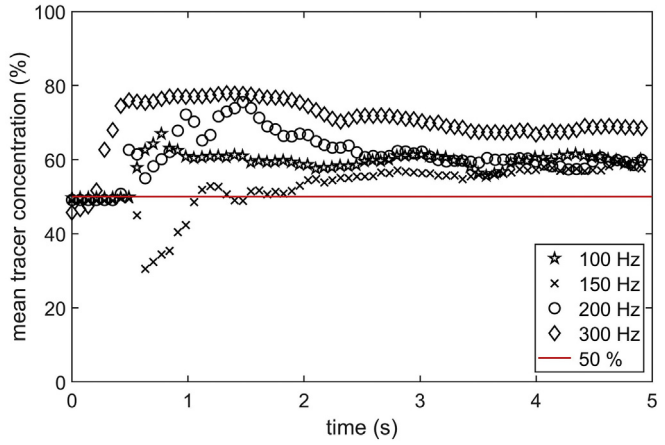

Fig. 16. Mean tracer concentration measured at the sampling spots indicated in Fig. 6 over mixing time. (For interpretation of the references to colour in this figure legend, the reader is referred to the web version of this article.)

segregated volume and located within it, no mixing can take place and therefore the mixing progress stagnates until the mixing zone hits the interface between two striations.

An evaluation of the overall mean of the sample spots is shown in Fig. 16. The initial values are close to 50% for all experiments, as one would expect based on the results of the calibration validation in Fig. 10. As soon as the mixing process starts, strong deviations from the mean in different directions are observed which is linked to the onset of agitation. Except for the 300 Hz experiment, the mean tracer concentration values converge to about 60%. A look at the images suggests that the deviation between the 300 Hz experiment and the others can be explained by the fact that most of the white powder is transported to the backside of the container in this experiment and is hence not visible. The deviation from 50% which the remaining experiments have in common are suspected to be linked to the abrasion of dye particles during the mixing process.

The fact that the mean concentration varies only an order of $\pm 5\%$ together with a high Lacey index indicates a steady homogeneous state for 100, 150 and 200 Hz after a mixing time of 3 s. As the 300 Hz experiment yields a Lacey index of only 0.85 and a mean concentration which is 10% off the other experiments' results after 5 s of mixing, 300 Hz vibration is not considered suitable for the chosen objectives.

4. Conclusion

The results of the present study suggest three key conclusions

- A single-tablet-scale mixing process was developed by exposing a powder bed to vibrations which led to agitation of the powder. Mixing performance was investigated for a variety of frequencies and amplitudes using a colored tracer, high-speed video recordings and image analysis. The high spatial and temporal resolution of the video recordings provided insights on the rate and quality of the mixing process.
- Vibratory mixing of pharmaceutical powders at acceleration magnitudes of ~112 g and frequencies of either 100 or 150 Hz leads to a high degree of homogeneity (Lacey index of ~0.95 and a close to constant mean concentration at the observable surface) after 2 s of mixing. The same can be said for 200 Hz and an acceleration magnitude of 102 g after 3 s. As our process aims at mixing of powders for a single tablet, the results satisfy the needs for homogeneity. The mixing process running at 300 Hz and 92 g did not deliver a satisfactory blend in the specified time.
- Within the investigated range, at similar levels of acceleration, lower frequencies and therefore higher amplitudes provide more efficient mixing. Due to our observations we propose a direct link between the size of the highly active mixing zones and the efficacy of a vibratory powder mixing process.
- Colorimetric analysis based on the evaluation of high-speed recordings is a valuable tool for continuous evaluation of the mixing quality within a small-scale vibratory mixer. This way of analysis allowed working with multiple sample spots in a small volume and without disturbance of the mixing process by drawing samples. The two mixing metrics calculated, i.e., the Lacey index and the maximum relative striation area both reflect the visually observable progress of the mixing process. The Lacey index occurred to be the more robust means of analysis, as it is not affected by fluctuations due to rupture and coalescence of continuous striation areas.

Fines, either present at the beginning of the mixing process or generated during it, potentially impact the outcome of an image-based concentration analysis. In future work a focus will be on this topic, to reduce the clouding effect of fines at the wall. Furthermore, a transient calibration could be applied with calibration standards mixed by a low shear mixing process, to keep the amount of fines at the level of the original powders. A first investigation should give insight if there is any difference in the generation of fines for different frequencies or accelerations.

As the investigated system of a 1:1 mixture is only representative for high dose APIs like Ibuprofen or ASA, further investigation on detection limits and accuracy for low doses should be done in the future. This should also include the use of different API and excipient powders. To improve the comparability between different frequencies, an acceleration control could be implemented to guarantee the same acceleration magnitude for different frequencies. This will also come into play when it comes to mass differences for future tests of different vessel geometries and fill levels. Investigations on the flow field within the powder bed using particle image velocimetry (PIV) would be useful as well. These could provide information about the size of highly active mixing zones and the velocities therein. Furthermore, the interface between dilute mixing zones and denser regions should be investigated in more detail to get insight in the particle transfer from areas with high density to the dilute mixing zones.

Role of the Funding Source

The present work was not sponsored by any external organization.

Declaration of Competing Interest

The authors declare that they have no known competing financial interests or personal relationships that could have appeared to influence the work reported in this paper.

Acknowledgements

The Authors acknowledge the support of the RCPE GmbH in terms of the supply of laboratory equipment, sample powders and execution of particle size measurements. Furthermore, we want to thank the team of the Vehicle Safety Institute of Graz University of Technology especially Alexander Hödl for the support in acquiring the high-speed image recordings.

Appendix A. Supplementary data

Supplementary data to this article can be found online at https://doi.org/10.1016/j.powtec.2021.04.040.

References

[1] P. Suri, S.V. Atre, R.M. German, J.P. de Souza, Effect of mixing on the rheology and particle characteristics of tungsten-based powder injection molding feedstock, Mater. Sci. Eng. A 356 (2003) 337–344.
[2] A. Gökçe, F. Fındık, A.O. Kurt, Microstructural examination and properties of premixed Al–Cu–Mg powder metallurgy alloy, Mater. Charact. 62 (2011) 730–735.

[3] B. Cuq, H. Berthiaux, C. Gatumel, Powder mixing in the production of food powders, in: B. Bhandari, M. Zhang, N. Bansal, P. Schuck (Eds.),Handbook of Food Powders. Processes and Properties 2013, pp. 200–229.
[4] I. Gijón-Arreortúa, A. Tecante, Mixing time and power consumption during blending of cohesive food powders with a horizontal helical double-ribbon impeller, J. Food Eng. 149 (2015) 144–152.
[5] M. Zebregs, A.E.H.J. Mayer, A.E.D.M. Heijden, Comparison of propellant processing by cast-cure and resonant acoustic mixing, Prop., Explos., Pyrotech 45 (2020) 87–91.
[6] A.U. Vanarase, J.G. Osorio, F.J. Muzzio, Effects of powder flow properties and shear environment on the performance of continuous mixing of pharmaceutical powders, Powder Technol. 246 (2013) 63–72.
[7] B. Chaudhuri, A. Mehrotra, F.J. Muzzio, M.S. Tomassone, Cohesive effects in powder mixing in a tumbling blender, Powder Technol. 165 (2006) 105–114.
[8] C.A. Radeke, B.J. Glasser, J.G. Khinast, Large-scale powder mixer simulations using massively parallel GPUarchitectures, Chem. Eng. Sci. 65 (2010) 6435–6442.
[9] S. Massol-Chaudeur, H. Berthiaux, J.A. Dodds, Experimental study of the mixing kinetics of binary pharmaceutical powder mixtures in a laboratory hoop mixer, Chem. Eng. Sci. 57 (2002) 4053–4065.
[10] A. Faure, P. York, R.C. Rowe, Process control and scale-up of pharmaceutical wet granulation processes: a review, Eur. J. Pharm. Biopharm. 52 (2001) 269–277.
[11] S. Poozesh, E. Bilgili, Scale-up of pharmaceutical spray drying using scale-up rules: a review, Int. J. Pharm. 562 (2019) 271–292.
[12] C. Vervaet, J.P. Remon, Continuous granulation in the pharmaceutical industry, Chem. Eng. Sci. 60 (2005) 3949–3957.
[13] M. Jivraj, L.G. Martini, C.M. Thomson, An overview of the different excipients useful for the direct compression of tablets, Pharm. Sci. Technol. Today 3 (2000) 58–63.
[14] C. Mao, V.R. Thalladi, D.K. Kim, S.H. Ma, D. Edgren, S. Karaborni, Harnessing ordered mixing to enable direct-compression process for low-dose tablet manufacturing at production scale, Powder Technol. 239 (2013) 290–299.
[15] M.A. Hamburg, F.S. Collins, The path to personalized medicine, N. Engl. J. Med. 363 (2010) 301–304.
[16] F.M. Franssen, P. Alter, N. Bar, B.J. Benedikter, S. Iurato, D. Maier, M. Maxheim, F.K. Roessler, M.A. Spruit, C.F. Vogelmeier, E.F. Wouters, B. Schmeck, Personalized medicine for patients with COPD: where are we? Int. J. Chronic Obstruct. Pulmonary Dis. 14 (2019) 1465–1484.
[17] I.M. Kronish, Y.K. Cheung, D. Shimbo, J. Julian, B. Gallagher, F. Parsons, K.W. Davidson, Increasing the precision of hypertension treatment through personalized trials: a pilot study, J. Gen. Intern. Med. 34 (2019) 839–845.
[18] T. Pullar, A.J. Birtwell, P.G. Wiles, A. Hay, M.P. Feely, Use of a pharmacologic indicator to compare compliance with tablets prescribed to be taken once, twice, or three times daily, Clin. Pharmacol. Ther. 44 (1988) 540–545.
[19] D.R. Bangsberg, K. Ragland, A. Monk, S.G. Deeks, A single tablet regimen is associated with higher adherence and viral suppression than multiple tablet regimens in HIV+ homeless and marginally housed people, AIDS (London, England) 24 (2010) 2835–2840.
[20] F. Puigventós, M. Riera, C. Delibes, M. Peñaranda, L.d. La Fuente, A. Boronat, Estudios de adherencia a los fármacos antirretrovirales, Una revisión sistemática, Medicina Clínica 119 (2002) 130–137.
[21] S. Lakio, T. Ervasti, P. Tajarobi, H. Wikström, M. Fransson, A.-P. Karttunen, J. Ketolainen, S. Folestad, S. Abrahmsén-Alami, O. Korhonen, Provoking an end-to-end continuous direct compression line with raw materials prone to segregation, Eur. J. Pharm. Sci. Off. J. Eur. Feder. Pharm. Sci. 109 (2017) 514–524.
[22] J.C. Samyn, K.S. Murthy, Experiments in powder blending and unblending, J. Pharm. Sci. 63 (1974) 370–375.
[23] M.J. Metzger, B. Remy, B.J. Glasser, All the Brazil nuts are not on top: vibration induced granular size segregation of binary, ternary and multi-sized mixtures, Powder Technol. 205 (2011) 42–51.
[24] R. Hogg, Mixing and segregation in powders: evaluation, mechanisms and processes, KONA 27 (2009) 3–17.
[25] P. Tang, V.M. Puri, Methods for minimizing segregation: a review, Part. Sci. Technol. 22 (2004) 321–337.
[26] H. Xiao, P.B. Umbanhowar, J.M. Ottino, R.M. Lueptow, Modelling density segregation in flowing bidisperse granular materials, Proc. R. Soc. A. 472 (2016) 20150856.
[27] G.G. Pereira, P.W. Cleary, Segregation due to particle shape of a granular mixture in a slowly rotating tumbler, Granular Matter 19 (2017).
[28] A. Jarray, H. Shi, B.J. Scheper, M. Habibi, S. Luding, Cohesion-driven mixing and segregation of dry granular media, Sci. Rep. 9 (2019) 13480.
[29] N. Harnby, An engineering view of pharmaceutical powder mixing, Pharm. Sci. Technol. Today 3 (2000) 303–309.
[30] M. Schröter, S. Ulrich, J. Kreft, J.B. Swift, H.L. Swinney, Mechanisms in the size segregation of a binary granular mixture, Phys. Rev. E Stat. Nonlinear Soft Matter Phys. 74 (2006) 11307.
[31] P. Eshuis, K. van der Weele, D. van der Meer, R. Bos, D. Lohse, Phase diagram of vertically shaken granular matter, Phys. Fluids 19 (2007) 123301.
[32] F. Zhang, L. Wang, C. Liu, P. Wu, S. Zhan, Patterns of convective flow in a vertically vibrated granular bed, Phys. Lett. A 378 (2014) 1303–1308.
[33] Resodyn Corporation, Resonant Acoustic Mixing - Technical White Paper, https://resodynmixers.com/download/resonantacoustic-mixing-technical-white-paper/.
[34] R. Tanaka, N. Takahashi, Y. Nakamura, Y. Hattori, K. Ashizawa, M. Otsuka, Verification of the mixing processes of the active pharmaceutical ingredient, excipient and lubricant in a pharmaceutical formulation using a resonant acoustic mixing technology, RSC Adv. 6 (2016) 87049–87057.
[35] G. Rátkai, Particle flow and mixing in vertically vibrated beds, Powder Technol. 15 (1976) 187–192.
[36] S.S. Hsiau, L.S. Lu, C.H. Tai, Experimental investigations of granular temperature in vertical vibrated beds, Powder Technol. 182 (2008) 202–210.
[37] J.G. Osorio, F.J. Muzzio, Evaluation of resonant acoustic mixing performance, Powder Technol. 278 (2015) 46–56.
[38] J.G. Osorio, K. Sowrirajan, F.J. Muzzio, Effect of resonant acoustic mixing on pharmaceutical powder blends and tablets, Adv. Powder Technol. 27 (2016) 1141–1148.
[39] R.W. Gerlach, J.M. Nocerino, Guidance for Obtaining Representative Laboratory Analytical Subsamples from Particulate Laboratory Samples, 2003.
[40] M. Asachi, E. Nourafkan, A. Hassanpour, A review of current techniques for the evaluation of powder mixing, Adv. Powder Technol. 29 (2018) 1525–1549.
[41] B.N. Asmar, P.A. Langston, A.J. Matchett, A generalised mixing index in distinct element method simulation of vibrated particulate beds, Granul. Matter 4 (2002) 129–138.
[42] P.M.C. Lacey, Developments in the theory of particle mixing, J. Appl. Chem. 4 (1954) 257–268.
[43] A. Kukukova, J. Aubin, S.M. Kresta, A new definition of mixing and segregation: three dimensions of a key process variable, Chem. Eng. Res. Des. 87 (2009) 633–647.
[44] A. Kukukova, J. Aubin, S.M. Kresta, Measuring the scale of segregation in mixing data, Can. J. Chem. Eng. 89 (2011) 1122–1138.
[45] J.G. Osorio, E. Hernández, R.J. Romañach, F.J. Muzzio, Characterization of resonant acoustic mixing using near-infrared chemical imaging, Powder Technol. 297 (2016) 349–356.
[46] R. Tanaka, N. Takahashi, Y. Nakamura, Y. Hattori, K. Ashizawa, M. Otsuka, In-line and real-time monitoring of resonant acoustic mixing by near-infrared spectroscopy combined with chemometric technology for process analytical technology applications in pharmaceutical powder blending systems, Anal. Sci. Int. J. Jpn. Soc. Anal. Chem. 33 (2017) 41–46.
[47] H.N. Emady, M. Wittman, S. Koynov, W.G. Borghard, F.J. Muzzio, B.J. Glasser, A.M. Cuitino, A simple color concentration measurement technique for powders, Powder Technol. 286 (2015) 392–400.
[48] S. Jaeger, M. Ehni, C. Eberhardt, M. Rolle, P. Grathwohl, G. Gauglitz, CCD camera image analysis for mapping solute concentrations in saturated porous media, Anal. Bioanal. Chem. 395 (2009) 1867–1876.
[49] O. Scheibelhofer, J. Kruisz, J. Rehrl, E. Faulhammer, A. Witschnigg, J.G. Khinast, LIF or dye: comparison of different tracing methods for granular solids, Powder Technol. 367 (2020) 20–31.
[50] R.C. Rowe (Ed.), Handbook of Pharmaceutical Excipients, 6th edAPhA (PhP) Pharmaceutical Press, London, 2009.
[51] F. Moisy, EzyFit 2.44, https://de.mathworks.com/matlabcentral/fileexchange/10176-ezyfit-2-44 2020 Accessed 24 July 2020.
[52] P. Bhalode, M. Ierapetritou, A review of existing mixing indices in solid-based continuous blending operations, Powder Technol. 373 (2020) 195–209.
[53] Z. Gu, J. Chen, A probabilistic analysis of some selected mixing indices, Chem. Eng. Res. Des. 93 (2015) 293–303.
[54] M. Rhodes, X. Wang, M. Nguyen, P. Stewart, K. Liffman, Study of mixing in gas-fluidized beds using a DEM model, Chem. Eng. Sci. 56 (2001) 2859–2866.
[55] P.Y. Liu, R.Y. Yang, A.B. Yu, DEM study of the transverse mixing of wet particles in rotating drums, Chem. Eng. Sci. 86 (2013) 99–107.